ACS APPLIED MATERIALS & INTERFACES

Research Article

Cite This: ACS Appl. Mater. Interfaces 2018, 10, 38558−38564

www.acsami.org

Mechanical Properties and Chemical Reactivity of Li_xSiO_y Thin Films

Yun Xu,[†] Caleb Stetson,[‡,§] Kevin Wood,[†] Eric Sivonxay,[∥] Chunsheng Jiang,[†] Glenn Teeter,[†] Svitlana Pylypenko,[§] Sang-Don Han,[‡] Kristin A. Persson,[∥,⊥] Anthony Burrell,[‡] and Andriy Zakutayev*,[†]

[†]Materials Science Center and [‡]Chemistry and Nanoscience Center, National Renewable Energy Laboratory, Golden, Colorado 80401, United States

[§]Department of Chemistry, Colorado School of Mines, Golden, Colorado 80401, United States

[∥]Lawrence Berkeley National Laboratory, Berkeley, California 94720, United States

[⊥]Department of Materials Science & Engineering, University of California, Berkeley, California 94720-1760, United States

Supporting Information

ABSTRACT: Silicon (Si) is a commonly studied candidate material for next-generation anodes in Li-ion batteries. A native oxide SiO_2 on Si is often inevitable. However, it is not clear if this layer has a positive or negative effect on the battery performance. This understanding is complicated by the lack of knowledge about the physical properties of the SiO_2 lithiation products and by the convolution of chemical and electrochemical effects during the anode lithiation process. In this study, Li_xSiO_y thin films as model materials for lithiated SiO_2 were deposited by magnetron sputtering at ambient temperature, with the goal of (1) decoupling chemical reactivity from electrochemical reactivity and (2) evaluating the physical and electrochemical properties of Li_xSiO_y. X-ray photoemission spectroscopy analysis of the deposited thin films demonstrate that a composition close to previous experimental reports of lithiated native SiO_2 can be achieved through sputtering. Our density functional theory calculations also confirm that the possible phases formed by lithiating SiO_2 are very close to the measured film compositions. Scanning probe microscopy measurements show that the mechanical properties of the film are strongly dependent on lithium concentration, with a ductile behavior at a higher Li content and a brittle behavior at a lower Li content. The chemical reactivity of the thin films was investigated by measuring the AC impedance evolution, suggesting that Li_xSiO_y continuously reacts with the electrolyte, in part because of the high electronic conductivity of the film determined from solid-state impedance measurements. The electrochemical cycling data of the sputter-deposited Li_xSiO_y/Si films also suggest that Li_xSiO_y is not beneficial in stabilizing the Si anode surface during battery operation, despite its favorable mechanical properties.

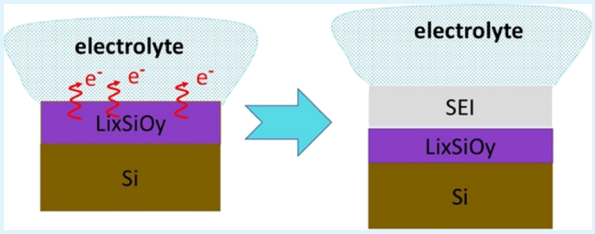

KEYWORDS: *mechanical properties, chemical reactivity, solid electrolyte interphases, Li_xSiO_y, lithium ion batteries*

INTRODUCTION

Silicon (Si) is considered to be one of the leading candidates for next-generation anode materials in Li-ion batteries, as it features a theoretical capacity more than 10 times higher than graphite.[1] However, one of the major challenges of silicon is the large volume change during the lithiation and delithiation processes. This volume change eventually leads to the breakdown of the solid electrolyte interphase (SEI) and further reactions that cause increased electrolyte consumption, higher interphase resistance, and the ultimate failure of the cell.[2]

There have been extensive studies on the SEI formation on the surface of silicon.[3] Although various reports on the overall composition of the SEI are reaching some consensus, the understanding of its physical properties and chemical reactivity is still limited. Most work is focused on the SEI composition through characterization by Fourier transform infrared reflectance and X-ray photoemission spectroscopy (XPS),[4−9] whereas less research has been done to separately study the SEI properties independent of the electrode.[10] Theoretically, a good SEI should be flexible or soft enough to accommodate the large volumetric change of the silicon. In addition to the mechanical properties of the SEI, high ionic conductivity and low electronic conductivity are also the important factors determining if a certain phase is beneficial to electrode stability.

It has been hypothesized that one of the most important SEI components for Si anodes in Li-ion batteries is Li_xSiO_y, which originates from the lithiation of the native oxide on Si (SiO_2). The role of SiO_2 on a Si anode is controversial: on one hand, it confines the volume expansion of Si, whereas on the other hand it induces interfacial reactions that consume lithium in the electrolyte. The lithiation of SiO_2 is a complicated process, and the products depend on the charge state of the battery.[11−13]

Received: July 2, 2018
Accepted: October 15, 2018
Published: October 15, 2018

DOI: 10.1021/acsami.8b10895
ACS Appl. Mater. Interfaces 2018, 10, 38558−38564

The general findings are that SiO_2 can be reduced to the possible products of $Li_2Si_2O_5$, Li_4SiO_4, Li_2O, Si, and Li_xSi.[10] Nevertheless, most of the recent model system studies are focused on the fully oxidized lithium silicates such as Li_4SiO_4, Li_2SiO_3, and $Li_2Si_2O_5$.[7,14−16]

In this work, the mechanical and electrochemical properties, as well as the chemical reactivity of the composite Li_xSiO_y film, are investigated. For this purpose, a special combinatorial Li_xSiO_y composite film with a composition close to that of the lithiated SiO_2 was synthesized by reactive sputtering, allowing to study its mechanical properties without any effect from the electrolyte decomposition products. According to the XPS results, both the lithium-rich and silicon-rich areas consist of lithium silicates, some Li_xSi_y, and very little SiO_2. The film compositions agree well with the phase diagram predicted by density functional theory (DFT) calculations. It is found that the composite Li_xSiO_y film exhibits a relatively high electronic conductivity and low hardness, based on the scanning probe microscopy (SPM) results and impedance measurements. The computed bulk moduli show the same trend as that of the experimental results, specifically that higher Li content leads to lower moduli. To evaluate the chemical reactivity of these materials, a multilayer thin-film Li_xSiO_y on Si was measured using impedance spectroscopy in a coin cell followed by electrochemical charge/discharge cycling. The results indicate that the composite film is unable to fully passivate the Si surface because of its high electronic conductivity and despite its ductile mechanical properties.

METHODS

Li_xSiO_y thin films were synthesized by radio frequency (RF) magnetron sputtering (13.56 MHz) using a lithium target (Lesker, 99.9%, 2″ diameter) and a silicon target (Lesker, 99.999%, 3″ diameter). The lithium target was cleaned with hexane (99.9%) before use to remove the residual mineral oil, which protects the lithium target from being oxidized during the shipment. Furthermore, the oxidized film on top of the lithium target was periodically removed by a Dremel tool with a copper brush. During the deposition, 30 W RF power was applied to both the lithium and silicon targets. Copper foil and EAGLE XG glass were used as substrates for the electrochemical measurement and SPM measurement, respectively. To generate plasma, Ar (99.999% purity) was introduced at a constant pressure of 3 mTorr into a vacuum chamber with a 3×10^{-8} Torr base pressure. The film was deposited at room temperature; so, it is expected to be amorphous (also confirmed by X-ray diffraction). After the synthesis, the samples were removed from the chamber to a glovebox. Airless transfer in a vacuum vessel to all characterization instruments was adopted because of the high reactivity of Li_xSiO_y. As a reference for comparison, thin films of Li-free Si and Li_xSiO_y/Si were made using the same method.

The XPS measurements were performed using a glovebox-integrated PHI 5600 XPS system. The glovebox conditions were better than <10 ppm moisture and O_2. The base pressure for the PHI 5600 XPS system was below 7×10^{-10} Torr. Photoelectrons were generated using monochromatic Al Kα X-ray excitation (1486.7 eV). The spectrometer binding energy (BE) scale was calibrated by measuring the valence-band and core-level spectra from sputter-cleaned Au, Ag, and Cu foils (EF = 0.00 eV, Au $4f_{7/2}$ = 83.96 eV, Ag $3d_{5/2}$ = 368.26 eV, and Cu $2p_{3/2}$ = 932.62 eV).[17] Ar^+ sputtering (incident energy of 3 keV) was used for depth profiling. Curve fitting and data processing were performed using Igor Pro with a custom program adapted from the literature.[18]

SPM techniques have been used to evaluate the mechanical and electrical properties of the thin films. Nanoindentation experiments were performed in an argon-filled glovebox with an atomic force microscope (Veeco D5000 and NanoScope V) using a Bruker DDESP diamond-coated Si probe in contact mode. Changing the deflection setpoints applied to the tip allows the force to be controlled based on the deflection versus z-distance calibration curves. For these experiments, four sites with different lithium concentrations were indented with varied indentation forces. Each indentation was held for a duration of 10 s. After unloading the indentation, tapping-mode atomic force microscopy (AFM) surface morphology images were taken and the indentation depths were measured.

The electrochemical properties were investigated by making coin cells and performing impedance spectroscopy measurement and galvanostatic cycling. The thin-film samples with 14 mm diameter were punched out from the silicon-rich region and lithium-rich region. The electrolyte was 1.2 M $LiPF_6$ in a 1:1 (volume) ethylene carbonate (EC) and dimethyl carbonate mixture. Lithium metal was used as the counter/reference electrode. The cells were first charged to 1.5 V (vs Li^+/Li hereafter) and then discharged to 50 mV. The impedance evolution was investigated by collecting the spectrums of a fresh electrode and an exposed electrode to an electrolyte for 24 h. The AC impedance data of a coin cell was collected in a frequency range of 100 kHz to 10 mHz. The solid-state AC impedance data of thin films deposited on interdigitated platinum electrodes were collected in a frequency range of 1 MHz to 1 Hz.

Phase stability was examined computationally by constructing a phase diagram from DFT calculations. The DFT calculations were performed, using the Vienna Ab-initio Simulation Package,[19,20] on known crystalline phases in the Li−Si−O system, found on the Materials Project.[19] The calculations were made using the projector augmented wave method with the generalized gradient approximation Perdew−Burke−Ernzerhof framework.[21,22] The structure optimization calculations allowed all the atomic positions and lattice parameters to relax. Plane-wave cutoff of 520 eV and a minimum reciprocal lattice k-point density of 64/Å^3 were used as parameters in DFT calculations. The Python Materials Genomics package (pymatgen) was used to construct the phase diagram of the Li_xSiO_y system.[23,24] Additionally, the bulk moduli were computed by fitting the Rose−Vinet equation[25] of state to the calculated energies and volumes of a series of deformed structures for the amorphous materials.

RESULTS AND DISCUSSION

Deposition and Characterization. High-throughput experimental combinatorial methods have been applied in materials science for the discovery and optimization of various functional materials.[26,27] These methods are also well-suited to electrochemical applications such as fuel cells and lithium-ion batteries.[28,29] In this work, a combinatorial approach was applied to screen the properties of lithium silicon compounds with different composition. The combinatorial chamber geometry is depicted in Figure 1. The lithium target was 8

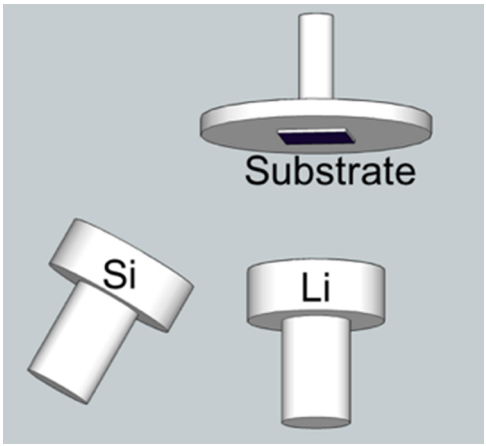

Figure 1. Chamber geometry used to deposit Li_xSiO_y thin films.

DOI: 10.1021/acsami.8b10895
ACS Appl. Mater. Interfaces 2018, 10, 38558−38564

cm away, facing the substrate, and the silicon target was 12 cm at an angle with respect to the substrate. Because of this geometry, the deposited films have a higher Si/Li ratio in the region closer to the silicon source and a lower Si/Li ratio in the region further from the silicon source. From these experiments, we found that the target-to-substrate distance has a strong effect on the oxygen content in the film: the shorter the target–substrate distance, the lower is the oxygen content. This trend can be explained by the decreased reaction of lithium plasma particles with the oxygen contaminants in the chamber resulting from H_2O base pressure. Further, the oxygen content in the film can be minimized by increasing the deposition rate by increasing the power applied to the Li and Si targets. However, the power applied to the Li target cannot be too high to avoid Li melting.

In Figure 2, depth profiles are shown for the Li 1s, Si 2p, and O 1s core-level spectra, for both the lithium-rich and silicon-rich regions of the thin film. From the XPS depth profile, significant oxidation was observed at the surface, even though the samples were protected from ambient atmosphere during the transfer from the deposition to the characterization instrument. Figure S1 shows the experimental spectra (and the corresponding peak fits) obtained from the bulk of the film. The compositions obtained via peak-fitting these spectra are listed in Table S1. As can be seen from the XPS fitting results in Table S1, for both the lithium-rich and silicon-rich sides of the film, lithium silicate and lithium silicide are the main components in the film, with some contribution from SiO_2. The average compositions for the lithium-rich and silicon-rich areas are $Li_{4.88}Si_{2.85}O_{2.52}$ and $Li_{1.58}Si_{1.31}O_{1.95}$, respectively. Hence, the thin film is subsequently referred to as a Li_xSiO_y composite film. We note that the lithium-rich area has more lithium and more O compared to the silicon-rich area. The higher oxygen content in the lithium-rich area results from the higher affinity of lithium to oxygen.

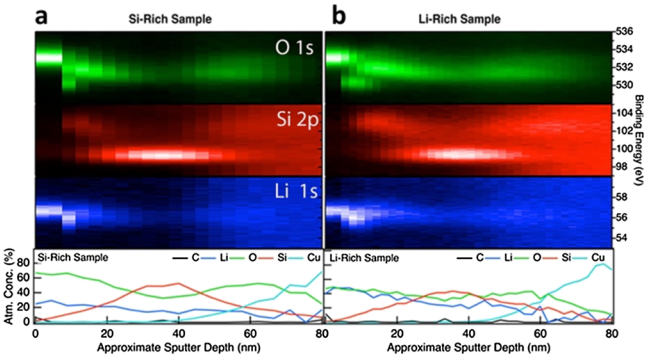

Figure 2. XPS depth profile analysis of the Li_xSiO_y composite thin film on copper foil for (a) Si-rich region and (b) Li-rich region. The top panels show the BE depth profile of O 1s (green), Si 2p (red), and Li 1s (blue). The bottom panel shows atomic percentage as a function of sputter depth.

The ternary phase diagram in Figure 3 shows the stability of crystalline compositions within the Li–Si–O phase space as predicted by DFT calculations. The nodes represent the compositions of stable crystalline phases, whereas the lines and triangles depict the two-phase and three-phase regions, respectively. The "phase diagram" of the amorphous structures is much more difficult to calculate, but it may be expected to be similar. Following the dashed line, the phase diagram predicts the possible lithiation products of SiO_2 to be lithium silicides, lithium silicates, and Li_2O depending on the degree of lithiation. For example, fully lithiated SiO_2 is predicted as a mixture of $Li_{21}Si_5$, Li, and Li_2O. The films studied in this work are amorphous according to X-ray diffraction and thus can be considered as the lithiation products of the amorphous SiO_2 layer on the Si surface. The observed lithium-rich and silicon-rich areas represent different lithiation stages of the SiO_2 film.

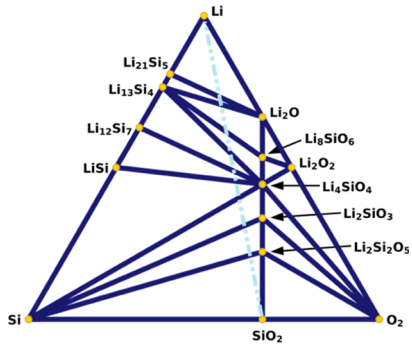

Figure 3. Phase diagram of the Li–Si–O_2 system at 0 K. The dashed blue line indicates the predicted lithiation trajectory from SiO_2.

Scanning Probe Microscopy. SPM-based nanoindentation measurements were performed on Li_xSiO_y thin films and a reference Si sample. The surface morphology is depicted in Figure S2a, indicating the film roughness of 20 nm in an area 0.5 μm by 0.5 μm. Figure S2b shows the typical residual indentation imprints of the film reflecting the film behavior upon different force loads.

The mechanical responses from the lithium-rich and silicon-rich Li_xSiO_y are shown in Figure 4a. In the lithium-rich area, a linear increase of indentation depth with the load was observed in a force range of 5–55 μN, indicating ductile behavior. In contrast, the silicon-rich area of Li_xSiO_y shows a brittle behavior: here, the probe easily broke through the film and the cracks propagated, independent of the load in the force range. Figure 4b shows a scan in AFM height mode of the six indentation points on both the silicon-rich and lithium-rich regions. The magnified images in both the height and phase AFM modes (Figure S3) also show the difference between the ductile and brittle behaviors.

To visualize the transition better, the indentation depth is plotted against the changing lithium concentration in the combinatorial sample in Figure S4. An inflection point, where the indentation depth increases sharply at a low Li content, is due to the cracking of the film in a brittle manner. The computational results for the different amorphous structure configurations (see Figure 5) confirm this trend: the higher lithium concentration both in Si and SiO_2 causes a decrease of the bulk moduli. We note that the film is composed of both lithium silicide and lithium silicates, and hence it combines the mechanical properties of both materials. Incidentally, the film composition falls close to the critical transition point of Li/Si = 1:1. The reference crystalline Si showed a very hard behavior, that is, the indentation depth is 0 nm.

Electrochemical Impedance and Cycling. To obtain further insights into the chemical reactivity of the Li_xSiO_y composite films, a 50 nm thick sample was assembled into a coin cell and investigated by impedance spectroscopy and by galvanostatic charge and discharge measurements (Figure 6). Capacity is not normalized in this work, as all the films have the same thickness and area. As shown in Figure 6a, a low amount

DOI: 10.1021/acsami.8b10895
ACS Appl. Mater. Interfaces 2018, 10, 38558−38564

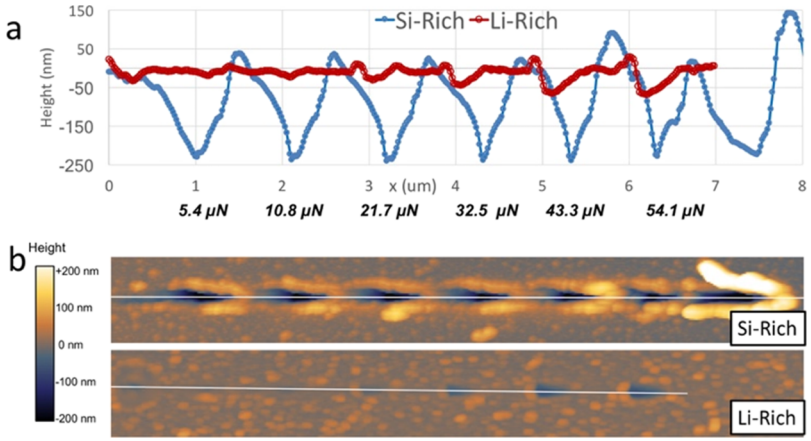

Figure 4. (a) Indentation depth at different sites with increasing indentation force aligned with each valley in the curve. (b) AFM images of indented film at both silicon-rich and lithium-rich regions.

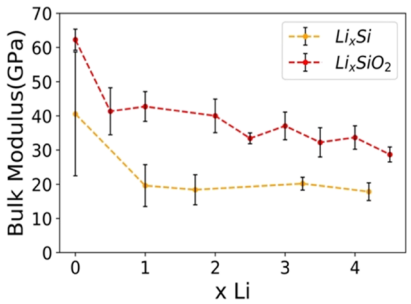

Figure 5. Calculated bulk moduli of lithiated silicon and lithiated SiO_2 plotted against the degree of lithiation of these amorphous structures. The error bars correspond to the different configurations of the amorphous structures.

of lithium could be extracted from the film even up to 1.5 V during the first charge cycle. This high open-circuit voltage (OCV) is due to the lower electrochemical potential of lithium in Li_xSiO_y which has a part of lithium bonded with oxygen. To investigate the reaction of the Li_xSiO_y composite film with an electrolyte, it was measured by AC impedance at the OCV, as shown in Figure 6b. When the Li_xSiO_y composite film comes into contact with the electrolyte, the charge-transfer resistance increases with time. In contrast, for the silicon electrode, the impedance is not time-dependent at OCV.

The higher charge-transfer resistance of Li_xSiO_y, as compared to Si, is likely to originate from the resulting Li_xSiO_y surface–electrolyte interface. The higher the lithium concentration in the compound, the lower will be the potential versus lithium, which promotes reduction reactions with the electrolyte. During charging, as SiO_2 is lithiated to Li_xSiO_y, this increased reactivity may lead to further consumption of the electrolyte if Li_xSiO_y is exposed and not fully covered with the other chemically stable electrolyte decomposition products. There has been a work in the literature[30] discussing the reduction mechanisms of EC on the lithium silicide surface, which identify different mechanisms depending on the degree of lithiation. A higher concentration of lithium was found to be more reactive because of the explicit interaction of EC molecules with Li^+ ions at the surface. In addition, recent experimental work by our group found that both lithium silicide and lithium silicate react with the electrolyte and form fluoride and carbonate species which are commonly seen in the SEI components.[31,32] Computational works also demonstrate that chemistry-dependent interaction happens on the surface of lithium silicide with the electrolyte.[33] We note that the increased lithiation of SiO_2 leads to an increased reactivity with the electrolyte and consumes lithium inventory.

Impedance of the as-prepared Li_xSiO_y thin film on an interdigitated electrode (without any electrolyte exposure) is shown in Figure S5. This thin film behaves like a pure resistor, which is mainly because of the existence of lithium silicide in

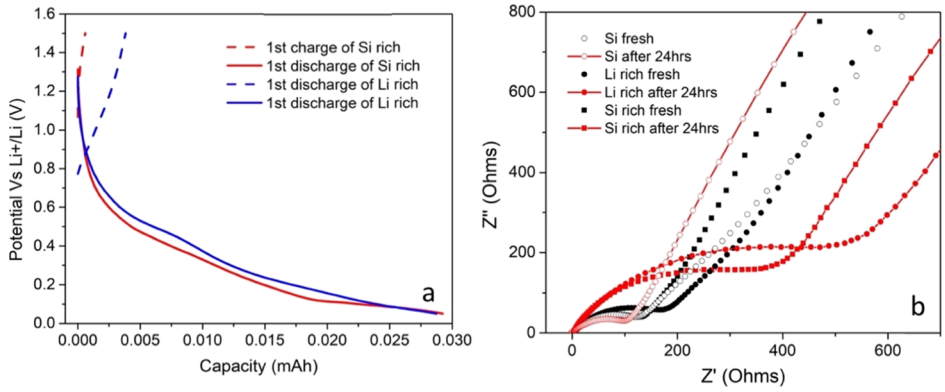

Figure 6. (a) Voltage profile of lithium-rich Li_xSiO_y composite film and silicon-rich Li_xSiO_y composite film. (b) Impedance evolution of lithium-rich Li_xSiO_y composite and silicon-rich Li_xSiO_y composite as well as Si film.

DOI: 10.1021/acsami.8b10895
ACS Appl. Mater. Interfaces 2018, 10, 38558−38564

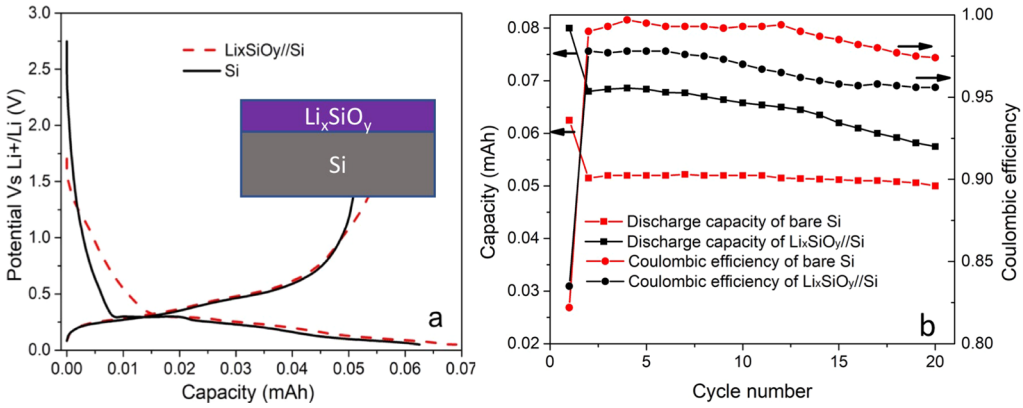

Figure 7. (a) Charge and discharge profiles of Si and Li_xSiO_y/Si, with the inset picture showing the schematic of a double-layer thin film. (b) Cycle performance and coulombic efficiency of double-layer thin film and pure silicon.

the film. Total conductivity is dominated by electronic conductivity. The total conductivity of a Li_xSiO_y thin film is calculated as

$$\sigma = L/(R \times A)$$

where σ is the conductivity, L is the distance between the Pt digits, and A is the total contacting area. The conductivity σ is calculated to be 2.7 S/cm, which is too high to be a good SEI layer.

To correlate the measured Li_xSiO_y properties with the electrochemical cycling performance of an electrode with Li_xSiO_y at the surface, a double-layer sample was deposited with Li_xSiO_y on top of a silicon thin film and compared to a Si film. The thickness of Li_xSiO_y was set to 10 nm to emulate the native oxide thickness, and the thickness of the silicon thin film was set to 50 nm, as shown in the inset in Figure 7a. As shown in Figure 7a, during the first cycle discharge profile, Li_xSiO_y/Si exhibited a lower OCV of only 1.5 V (compared to 2.5 V for Si) because of the existing lithium on the silicon surface. The difference of the CV profiles above 0.25 V (before Si starts lithiating) results from the surface reaction between Li_xSiO_y and the electrolyte. Both the low potential of Li_xSiO_y and its reaction products make the electrochemical reduction different from that in the silicon case. The lower potential range profiles for both films are very similar, as the same thickness of the silicon film was deposited. The cycling of Li_xSiO_y/Si showed a lower coulombic efficiency and less stable performance as compared to that of the bare silicon (see Figure 7b). We note that the coulombic efficiency of silicon is higher than that of the Li_xSiO_y-coated Si, indicating that the Li_xSiO_y film exhibits a greater reactivity with the electrolyte. We hypothesize that the Li_xSiO_y composite film continuously reacts with the electrolyte, preventing the stabilization of SEI on the silicon electrode. These results suggest that SiO_2 does not help stabilize the surface of the Si electrode, as the lithiation products are not stable upon cycling. Previously, there has been a study[34] on the effect of SiO_2 with various thicknesses from 2, 7, to 10 nm on the anode performance of silicon nanowires. Only the 7 nm SiO_2-coated Si showed an improved performance compared to Si. This is a complementary result from both mechanical property and reactivity. More studies of the reaction product between Li_xSiO_y and the electrolyte are in progress to clarify the role of Li_xSiO_y in the functionality and SEI stabilization of the Si anode.

CONCLUSIONS

In summary, the mechanical and electrochemical properties, as well as the chemical reactivity, of the Li_xSiO_y composite thin film with the Li-to-Si ratio between 1.7 and 1.1 were investigated. These Li_xSiO_y films with Li-rich and Si-rich compositions were prepared by combinatorial sputtering as a model system to study the initial products of lithiation of native oxide SiO_2 layer on a Si anode, relevant for next-generation Li-ion batteries. The first-principles computational results show that the behavior of both lithiated silicon and lithiated SiO_2 transition from brittle to ductile as lithiation happens. The as-synthesized composite Li_xSiO_y film, which is a mixture of lithium silicides and lithium silicates, shows an equivalent brittle-to-ductile transition. The intermediate product of lithiated SiO_2, which contains lithium silicates and lithium silicates, is highly reactive with the electrolyte because of the low potential resulting from the high lithium content. These composite Li_xSiO_y with Li/Si = 1.7 and 1.1 showed a low electronic resistance and did not facilitate the passivation and stabilization of the Si films, despite their low resistance to fracture. Thus, a favorable ductile mechanical property is found to be a desirable but insufficient criterion for stable SEI formation; low chemical reactivity and low electronic conductivity are also important for stable electrodes.

ASSOCIATED CONTENT

Supporting Information

The Supporting Information is available free of charge on the ACS Publications website at DOI: 10.1021/acsami.8b10895.

XPS spectrum, AFM images, and impedance data (PDF)

AUTHOR INFORMATION

Corresponding Author

*E-mail: Andriy.Zakutayev@nrel.gov.

ORCID

Yun Xu: 0000-0002-6680-519X
Chunsheng Jiang: 0000-0003-0230-7500
Svitlana Pylypenko: 0000-0001-7982-734X
Sang-Don Han: 0000-0002-2931-659X
Kristin A. Persson: 0000-0003-2495-5509
Andriy Zakutayev: 0000-0002-3054-5525

DOI: 10.1021/acsami.8b10895
ACS Appl. Mater. Interfaces 2018, 10, 38558−38564

Author Contributions

The manuscript was written through contributions of all authors. All authors have given approval to the final version of the manuscript.

Notes

The authors declare no competing financial interest.

■ ACKNOWLEDGMENTS

This work was authored by the National Renewable Energy Laboratory, operated by Alliance for Sustainable Energy, LLC, for the U.S. Department of Energy (DOE) under contract no. DE-AC36-08GO28308. Funding provided by Vehicle Technologies Office, Hybrid Electric Systems Program. David Howell (Manager), Battery R&D, Brian Cunningham and Peter Faguy (Technology Managers), at the U.S. Department of Energy, Office of Energy Efficiency and Renewable Energy, are gratefully acknowledged. A portion of the research was performed using computational resources sponsored by the Department of Energy's Office of Energy Efficiency and Renewable Energy and located at the National Renewable Energy Laboratory. Computational resources of the National Energy Research Scientific Computing Center (NERSC), a U.S. Department of Energy Office of Science User Facility operated under contract no. DE-AC02-05CH11231, are gratefully acknowledged. The views expressed in the article do not necessarily represent the views of the DOE or the U.S. Government.

■ REFERENCES

(1) Franco Gonzalez, A.; Yang, N.-H.; Liu, R.-S. Silicon Anode Design for Lithium-Ion Batteries: Progress and Perspectives. *J. Phys. Chem. C* **2017**, *121*, 27775−27787.

(2) Zhu, J.; Wang, T.; Fan, F.; Mei, L.; Lu, B. Atomic-Scale Control of Silicon Expansion Space as Ultrastable Battery Anodes. *ACS Nano* **2016**, *10*, 8243−8251.

(3) Cheng, X.-B.; Zhang, R.; Zhao, C.-Z.; Wei, F.; Zhang, J.-G.; Zhang, Q. A Review of Solid Electrolyte Interphases on Lithium Metal Anode. *Adv. Sci.* **2016**, *3*, 1500213.

(4) Xu, W.; Wang, J.; Ding, F.; Chen, X.; Nasybulin, E.; Zhang, Y.; Zhang, J.-G. Lithium metal anodes for rechargeable batteries. *Energy Environ. Sci.* **2014**, *7*, 513−537.

(5) Aurbach, D. Review of selected electrode-solution interactions which determine the performance of Li and Li ion batteries. *J. Power Sources* **2000**, *89*, 206−218.

(6) Xu, K. Electrolytes and Interphases in Li-Ion Batteries and Beyond. *Chem. Rev.* **2014**, *114*, 11503−11618.

(7) Yang, C. R.; Wang, Y. Y.; Wan, C. C. Composition Analysis of the Passive Film on the Carbon Electrode of a Lithium-ion Battery with an EC-based Electrolyte. *J. Power Sources* **1998**, *72*, 66−70.

(8) Young, B. T.; Heskett, D. R.; Nguyen, C. C.; Nie, M.; Woicik, J. C.; Lucht, B. L. Hard X-ray Photoelectron Spectroscopy (HAXPES) Investigation of the Silicon Solid Electrolyte Interphase (SEI) in Lithium-Ion Batteries. *ACS Appl. Mater. Interfaces* **2015**, *7*, 20004−20011.

(9) Lindgren, F.; Xu, C.; Niedzicki, L.; Marcinek, M.; Gustafsson, T.; Björefors, F.; Edström, K.; Younesi, R. SEI Formation and Interfacial Stability of a Si Electrode in a LiTDI-Salt Based Electrolyte with FEC and VC Additives for Li-Ion Batteries. *ACS Appl. Mater. Interfaces* **2016**, *8*, 15758−15766.

(10) Weadock, N.; Varongchayakul, N.; Wan, J.; Lee, S.; Seog, J.; Hu, L. Determination of mechanical properties of the SEI in sodium ion batteries via colloidal probe microscopy. *Nano Energy* **2013**, *2*, 713−719.

(11) Dupré, N.; Moreau, P.; De Vito, E.; Quazuguel, L.; Boniface, M.; Bordes, A.; Rudisch, C.; Bayle-Guillemaud, P.; Guyomard, D. Multiprobe Study of the Solid Electrolyte Interphase on Silicon-Based Electrodes in Full-Cell Configuration. *Chem. Mater.* **2016**, *28*, 2557−2572.

(12) Zhao, J.; Lee, H.-W.; Sun, J.; Yan, K.; Liu, Y.; Liu, W.; Lu, Z.; Lin, D.; Zhou, G.; Cui, Y. Metallurgically lithiated SiOxanode with high capacity and ambient air compatibility. *Proc. Natl. Acad. Sci. U.S.A.* **2016**, *113*, 7408−7413.

(13) Zhang, Y.; Li, Y.; Wang, Z.; Zhao, K. Lithiation of SiO2 in Li-Ion Batteries: In Situ Transmission Electron Microscopy Experiments and Theoretical Studies. *Nano Lett.* **2014**, *14*, 7161−7170.

(14) Radvanyi, E.; De Vito, E.; Porcher, W.; Jouanneau Si Larbi, S. An XPS/AES Comparative Study of the Surface Behaviour of Nano-silicon Anodes for Li-ion Batteries. *J. Anal. At. Spectrom.* **2014**, *29*, 1120−1131.

(15) Philippe, B.; Dedryvère, R.; Gorgoi, M.; Rensmo, H.; Gonbeau, D.; Edström, K. Role of the LiPF6 Salt for the Long-Term Stability of Silicon Electrodes in Li-Ion Batteries - A Photoelectron Spectroscopy Study. *Chem. Mater.* **2013**, *25*, 394−404.

(16) Delpuech, N.; Mazouzi, D.; Dupré, N.; Moreau, P.; Cerbelaud, M.; Bridel, J. S.; Badot, J.-C.; De Vito, E.; Guyomard, D.; Lestriez, B.; Humbert, B. Critical Role of Silicon Nanoparticles Surface on Lithium Cell Electrochemical Performance Analyzed by FTIR, Raman, EELS, XPS, NMR, and BDS Spectroscopies. *J. Phys. Chem. C* **2014**, *118*, 17318−17331.

(17) Seah, M. P.; Gilmore, I. S.; Beamson, G. XPS: binding energy calibration of electron spectrometers 5?re-evaluation of the reference energies. *Surf. Interface Anal.* **1998**, *26*, 642−649.

(18) Schmid, M.; Steinrück, H.-P.; Gottfried, J. M. A new asymmetric Pseudo-Voigt function for more efficient fitting of XPS lines. *Surf. Interface Anal.* **2014**, *46*, 505−511.

(19) Jain, A.; Ong, S. P.; Hautier, G.; Chen, W.; Richards, W. D.; Dacek, S.; Cholia, S.; Gunter, D.; Skinner, D.; Ceder, G.; Persson, K. A. Commentary: The Materials Project: A materials genome approach to accelerating materials innovation. *APL Mater.* **2013**, *1*, 011002.

(20) Kresse, G.; Furthmüller, J. Efficient iterative schemes forab initiototal-energy calculations using a plane-wave basis set. *Phys. Rev. B: Condens. Matter Mater. Phys.* **1996**, *54*, 11169−11186.

(21) Blöchl, P. E. Projector Augmented-wave Method. *Phys. Rev. B: Condens. Matter Mater. Phys.* **1994**, *50*, 17953−17979.

(22) Perdew, J. P.; Burke, K.; Ernzerhof, M. Generalized Gradient Approximation Made Simple. *Phys. Rev. Lett.* **1996**, *77*, 3865−3868.

(23) Ong, S. P.; Wang, L.; Kang, B.; Ceder, G. Li−Fe−P−O2 Phase Diagram from First Principles Calculations. *Chem. Mater.* **2008**, *20*, 1798−1807.

(24) Ong, S. P.; Richards, W. D.; Jain, A.; Hautier, G.; Kocher, M.; Cholia, S.; Gunter, D.; Chevrier, V. L.; Persson, K. A.; Ceder, G. Python Materials Genomics (pymatgen): A robust, open-source python library for materials analysis. *Comput. Mater. Sci.* **2013**, *68*, 314−319.

(25) Vinet, P.; Smith, J. R.; Ferrante, J.; Rose, J. H. Temperature Effects on the Universal Equation of State of Solids. *Phys. Rev. B: Condens. Matter Mater. Phys.* **1987**, *35*, 1945−1953.

(26) Green, M. L.; Takeuchi, I.; Hattrick-Simpers, J. R. Applications of high throughput (combinatorial) methodologies to electronic, magnetic, optical, and energy-related materials. *J. Appl. Phys.* **2013**, *113*, 231101.

(27) Green, M. L.; Choi, C. L.; Hattrick-Simpers, J. R.; Joshi, A. M.; Takeuchi, I.; Barron, S. C.; Campo, E.; Chiang, T.; Empedocles, S.; Gregoire, J. M.; Kusne, A. G.; Martin, J.; Mehta, A.; Persson, K.; Trautt, Z.; Van Duren, J.; Zakutayev, A. Fulfilling the Promise of the Materials Genome Initiative with High-throughput Experimental Methodologies. *Appl. Phys. Rev.* **2017**, *4*, 011105.

(28) Muster, T. H.; Trinchi, A.; Markley, T. A.; Lau, D.; Martin, P.; Bradbury, A.; Bendavid, A.; Dligatch, S. A review of high throughput and combinatorial electrochemistry. *Electrochim. Acta* **2011**, *56*, 9679−9699.

(29) Carey, G. H.; Dahn, J. R. Combinatorial Synthesis of Mixed Transition Metal Oxides for Lithium-Ion Batteries. *ACS Comb. Sci.* **2011**, *13*, 186−189.

DOI: 10.1021/acsami.8b10895
ACS Appl. Mater. Interfaces 2018, 10, 38558−38564

(30) Martinez de la Hoz, J. M.; Leung, K.; Balbuena, P. B. Reduction Mechanisms of Ethylene Carbonate on Si Anodes of Lithium-Ion Batteries: Effects of Degree of Lithiation and Nature of Exposed Surface. *ACS Appl. Mater. Interfaces* **2013**, *5*, 13457−13465.
(31) Jaclyn Coyle, M. B. Christopher Apblett, Conrad Stoldt Investigating Chemical Reactivity of Lithium Silicate Model SEI Layers. In preparation.
(32) Xu, K. W. Y.; Coyle, J.; Engtrakul, C.; Teeter, G.; Conrad, S.; Burrell, A.; Zakutayev, A. Early Stage Solid Electrolyte Interphase Formation on Lithium Lilicide. In preparation.
(33) Martinez de la Hoz, J. M.; Soto, F. A.; Balbuena, P. B. Effect of the Electrolyte Composition on SEI Reactions at Si Anodes of Li-Ion Batteries. *J. Phys. Chem. C* **2015**, *119*, 7060−7068.
(34) Sim, S.; Oh, P.; Park, S.; Cho, J. Critical Thickness of SiO2Coating Layer on Core@Shell Bulk@Nanowire Si Anode Materials for Li-Ion Batteries. *Adv. Mater.* **2013**, *25*, 4498−4503.

DOI: 10.1021/acsami.8b10895
ACS Appl. Mater. Interfaces 2018, 10, 38558−38564